Modeling and Simulation Improvement in Laser Shock Processing

Wenwu Zhang and Y. Lawrence Yao
Department of Mechanical Engineering
Columbia University, New York, NY 10027

Abstract

Previous work has reported numerical and experimental results pertaining micro-scale laser shock processing, which imparts compressive residual stresses in metallic targets with higher spatial resolution. In this paper, the more detailed physical process of laser-liquid-solid interaction is considered to achieve more accurate simulation results of shock pressure and to provide values for coefficients which otherwise need to be arbitrarily chosen. The expansion of plasma is modeled as one-dimensional laser supported combustion wave. The 1D results are then modified to consider radial and axial expansion effects. The influence of pulse duration and beam size is also considered. Three-dimensional simulation of shock pressure-solid interaction is carried out as opposed to axisymmetric simulation reported previously. Finite extent of target geometry is also considered as opposed to the semi-infinite geometry assumed previously. The model and simulation improvement is experimentally validated.

1. Introduction

The expanding applications of micro devices make the mechanical properties of such devices an increasing concern. Processes that can improve the mechanical properties at micro scale are required. Laser Shock Processing (LSP) has been used to improve the hardness, fatigue life and residual stress distributions of metals at mm scale (Claurer, et al., 1981; Peyre et al., 1995; Berthe, et al., 1998). Laser shock processing of aluminum and copper at micro-scale has been studied in previous papers (Zhang and Yao, 2000a & b). This paper continues the study of micro-scale LSP, reporting improvements in modeling, simulation and experimental validation.

Efforts have been made in shock pressure modeling by Claurer et al. (1981), Fabbro et al. (1990) and Zhang and Yao (2000a & b). Previous models assume that a certain amount of plasma exists instantaneously once laser is on. A constant fraction of plasma internal energy is assumed to increase the pressure of the plasma. The value of this constant, α, has to be decided indirectly from back velocity measurement or arbitrarily chosen, and it varies from 0.1 to 0.4 in literature. The reason is that in previous models there is no consideration of mass exchanges between plasma and water or plasma and the ablated coating layer over the target metal, only energy and momentum conservation are considered. In reality, there are mass exchanges from water and coating layer into plasma. A model considering these physical processes has the potential to represent the process dynamics more realistically, which, along with the spatial distribution of the shock pressure, is important for the micro-scale LSP.

The dynamic deformation process of the target under the action of shock load had been simulated using finite element method (FEM), but only 1D flat plate case (Claurer, et al., 1981; Peyre et al., 1995; Berthe, et al., 1998) and 2D axisymmetric round disc case (Zhang and Yao, 2000a & b) were studied. In both cases, semi-infinite boundary conditions were implicitly assumed. Effects of finite size and complex geometry are important in practice, especially for LSP of small components and LSP near the edges of the components. In this paper, the expansion of plasma is modeled as 1D laser supported combustion wave. The 1D results are then modified to consider spatial expansion effects. Copper and nickel samples were processed using micro-scale LSP. The improvement of the new model is validated by comparing the predicted and measured deformation of the shocked samples.

2. Modeling of Laser Induced Shock Waves

When a high intensity laser beam is irradiated on a solid surface, the solid target vaporizes into plasma due to direct laser irradiation and plasma thermal coupling. Shock waves are induced as a result of the fast expansion of the plasma. If laser energy is not high enough or if the confining medium (air or water, etc.) is too dense as in the case of LSP (water confinement), the speed of plasma expansion is lower than the shock speed, thus shock wave proceeds plasma expansion. This is the case of laser supported combustion (LSC) wave (Root, 1989). Detailed modeling of laser shock processing should be based on physical laws of LSC wave. LSC wave in air and vacuum has been studied (Pirri et al., 1978) assuming that all laser energy is absorbed by the plasma, but modeling work of LSC wave in LSP configuration was not found. This paper extends the LSC model to water confined laser shock processing, and the laser energy is assumed to be partially absorbed by the plasma, which is more practical.

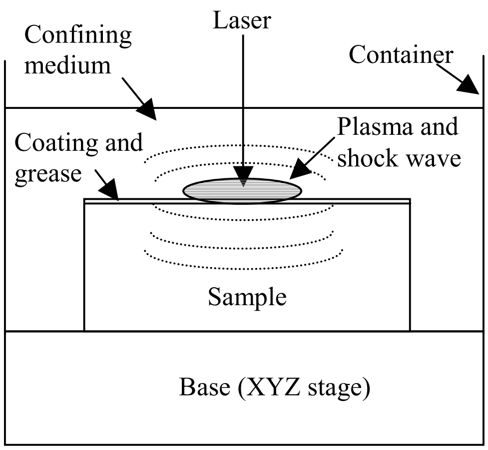

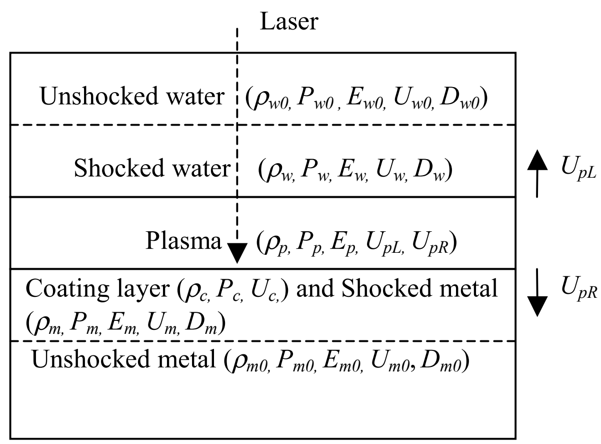

Figure 1 (a) Experimental setup of laser shock processing (LSP); and (b) Five regions in water confined LSP modeling.

Water is transparent to the laser beam if laser intensity is below the breakdown level at the wavelength used. Water converts into plasma due to plasma and laser induced water breakdown (Vogel, et al., 1996). For UV lasers at $\lambda = 355$nm, the breakdown level is around 4 GW/cm^2 (Berthe, et al., 1998). In LSP using water as confining medium (Fig. 1 (a)), laser irradiation vaporizes the coating layer of the solid target, and the vaporized material quickly evolves into plasma. Water near the plasma outer edge is quickly ionized and becomes strongly absorbent to incident laser irradiation. Thus water is changed into plasma due to plasma irradiation and direct laser irradiation. The pressure of the plasma increases quickly and the expansion of the plasma imparts shock pressure into water and target. Mass, momentum and energy are conserved across the shock wave. To model this process, the following assumptions are made:

(1) The early stage of plasma expansion is one-dimensional, i.e., plasma expands only in the axial direction. Density, internal energy and pressure of the plasma are uniform within the plasma volume but can vary with time. Particle velocity of the plasma changes linearly from the

water-plasma interface to the plasma-solid interface; (2) Plasma obeys ideal gas laws and absorbs a constant fraction of laser irradiation energy; (3) Only the coating layer is vaporized, the metal target experiences negligible thermal effects. The melting layer, Knudsen layer and the transition region from vapor to plasma of the coating layer are so thin that the thickness is negligible compared with the thickness of plasma. Their influence can be represented by the phase change energy in the energy conservation relation; (4) The coating layer is thin and well coupled with the metal target, thus the shock pressure and the particle velocity of the coating layer and the metal target are equal.

Let subscripts *w* denote water, *m* metal, *c* the coating layer, *p* plasma, *L* the side of plasma near water, *R* the side of plasma near solid, and *0* the property of unshocked region. Also let *D* be shock velocity, *U* particle velocity, *E* internal energy, ρ density, *P* pressure. For convenience, the water-plasma-target system is divided into five regions (Fig. 1(b)): unshocked water (ρ_{w0}, P_{w0}, E_{w0}, U_{w0}, D_{w0}), shocked water (ρ_w, P_w, E_w, U_w, D_w), plasma (ρ_p, P_p, E_p, U_{pL}, U_{pR}), coating layer and shocked solid (ρ_c, P_c, U_c, ρ_m, P_m, E_m, U_m, D_m), and unshocked solid (ρ_{m0}, P_{m0}, E_{m0}, U_{m0}, D_{m0}). The unshocked properties are known. All the unknowns are functions of time.

The shocked and unshocked properties of water are related by mass, momentum, and energy conservation, and shock speed constitutive relations:

$$\rho_{w0} / \rho_w = 1 - (U_w - U_{w0}) / (D_w - U_{w0}) \quad (1)$$

$$P_w - P_{w0} = \rho_{w0} (D_w - U_{w0})(U_w - U_{w0}) \quad (2)$$

$$(E_w + U_w^2 / 2) - (E_{w0} + U_{w0}^2 / 2) = \frac{1}{2}(P_w + P_{w0})(\frac{1}{\rho_{w0}} - \frac{1}{\rho_w}) \quad (3)$$

$$D_w = D_{w0} + S_w U_w \quad (4)$$

For water, U_{w0} = 0 m/s, P_{w0} = 10^5 Pa, E_{w0} = 0 J/kg, ρ_{w0}=997.9 kg/m^3, D_{w0}=2393 m/s, and S_w=1.333 (Assay and Shahinpoor, 1992). S_w is the coefficient relating particle velocity and shock velocity of water, while D_{w0} is the shock speed at infinitesimal particle speed.

Replacing subscript *w* with *m* in Eq. 1-4, one gets the relations between shocked and unshocked properties of metals (Eq. 5-8). U_{m0} = 0 m/s, P_{m0} = 10^5 Pa, E_{m0} = 0 J/kg. For copper, ρ_{m0}=8939 kg/m^3, D_{m0}=3933 m/s, and S_m=1.489. For nickel, ρ_{m0}=8874 kg/m^3, D_{m0}=4581 m/s, and S_m=1.463 (Meyers and Murr, 1981).

The above 8 equations can be solved after considering water and coating layer interactions with plasma. Mass and momentum conservations at the interfaces at any instant require:

$$\rho_w (U_{pL} - U_w) = \rho_p U_{pL} \quad (9)$$

$$\rho_c (U_{pR} - U_c) = \rho_c Vrec = \rho_p U_{pR} \quad (10)$$

$$P_p + \rho_p U_{pL} U_w = P_w \quad (11)$$

$$P_p + \rho_p U_{pR} U_c = P_c \quad (12)$$

The mass flow from water is $MF_w = \rho_w (U_{pL} - U_w)$. The mass flow from the coating layer is $MF_c = \rho_c (U_{pR} - U_c) = \rho_c Vrec$, where $Vrec$ is the recess velocity of the melting coating surface relative to the coating layer itself. In this paper, the coating layer is aluminum foil, ρ_c = 2700 Kg/m^3. According to assumption 4, U_m = U_c and P_m = P_c. The current mass of plasma is equal to the integration of the mass flows into plasma:

$$\rho_P (t) \int_0^t (U_{pL} + U_{pR}) dt = \int_0^t (MF_w + MF_c) dt \quad (13)$$

The energy conservation of plasma should consider the absorption of incident laser irradiation, the total energy stored in the plasma (E_{pt}), the work done by the plasma, and the energy exchanges through mass flows. E_{pt} consists of kinetic energy and internal energy. Based on the assumption of linear distribution of particle velocity, the unit mass kinetic energy of plasma is $E_{pk} = (U_{pL}^2 + U_{pR}^2 - U_{pL}U_{pR})/6$. Using the ideal gas law, the internal energy of plasma is related to its density, specific heat ratio γ (about 1.3), and pressure:

$$E_p = \frac{\gamma P_p}{(\gamma - 1)\rho_p} \tag{14}$$

So the total energy in plasma is $E_{pt} = \rho_p L(E_{pk} + E_p)$, where $L(t) = \int_0^t (U_{pL} + U_{pR})dt$ is the plasma length. The total work done by plasma to the surrounding is $W_p = \int_0^t P_p (U_{pL} + U_{pR})dt$.

The mass exchange induced energy exchange equals mass flow times the energy difference:

$$E_{MF} = \int_0^t [MF_c(E_{pk} + E_p - U_c^2/2 - Q_c) + MF_w(E_{pk} + E_p - U_w^2/2 - Q_w)]dt,$$

where Q_w and Q_c are the phase change energy of water and coating layer, respectively. The internal energy is incorporated into the phase change item.

Let AP be the fraction of laser energy absorbed by plasma, which may be experimentally determined but is taken as a constant in this paper for simplicity, $I(t)$ be the laser intensity, then the energy conservation of plasma requires:

$$E_{pt} + W_p - E_{MF} = \int_0^t AP \times I(t)dt \tag{15}$$

Now the equations of this 1D model are closed and all the variables involved can be solved as a function of time. Once plasma is created, radial expansion of plasma commences. A rarefaction wave propagates into the plasma from the edge at the sound speed of the plasma. After a characteristic time $T_r = R_0/a$, where R_0 is the radius of the laser beam and $a$is the sound speed of the plasma, the rarefaction wave coalesces at the center of the spot, and the pressure of the plasma drops and deviates from the 1D values. Axial relaxation starts after the laser pulse terminates, thus the characteristic time for axial expansion is $T_z = T_p$, where T_p is pulse duration. The temporal evolution of the plasma depends on the value of the T_r and T_z. Based on the work of Pirri (1978), Simons (1984), and Root (1989), the following power scaling laws are used in this paper.

Case 1: $T_r < T_z$, radial relaxation happens earlier than axial relaxation

$t < T_r$ $\quad P = P_{1D}, R = R_0$

$T_z > t > T_r$ $\quad P = P_{1D}(t/T_r)^{-4/5}, R = R_0(t/T_r)^{1/2}$

$t > T_z$ $\quad P = P_{1D}(T_r/T_z)^{4/5}(T_z/t)^{6/5}, R = R_0(T_z/T_r)^{1/2}(T_z/t)^{-4/5}$ (16)

Case 2: $T_r > T_z$, axial relaxation happens earlier than radial relaxation

$t < T_z$ $\quad P = P_{1D}, R = R_0$

$T_r > t > T_z$ $\quad P = P_{1D}(t/T_z)^{-3/2}, R = R_0$

$t > T_r$ $\quad P = P_{1D}(T_z/T_r)^{3/2}(T_r/t)^{6/5}, R = R_0(T_r/t)^{-2/5}$ (17)

where P_{1D} is the plasma pressure from 1D model described above. For the laser used in current research, $R_0 = 6$ microns, $T_z = T_p = 50$ ns, and sound speed of plasma $a = 300$ m/s, $T_r = 20$ ns, thus radial relaxation occurs earlier than axial relaxation (Case 1).

For laser shock processing in micro scale, the spatial profile of the laser beam should also be considered. Following the work of Zhang and Yao (2000a), shock pressure obeys Gaussian spatial distribution, but with its $1/e^2$ radius equals to $\sqrt{2}R(t)$, where $R(t)$ is the radius of plasma in Eq. 16. Let r be the radial distance from the center of the laser beam, the spatially uniform shock pressure $P(t)$ relates to the spatially non-uniform shock pressure as

$$P(r,t) = P(t)\exp\left(-\frac{r^2}{2R^2(t)}\right) \tag{18}$$

where r is the radial distance from the center of the laser beam.

3. Experimental and Simulation Conditions

Micro-scale LSP can be applied to a wide variety of metals. Copper and nickel are chosen in this study because the mechanical properties of nickel and copper differ, and they are often etched and deposited on silicon substrates as part of micro devices. Nickel is also used as a metallic MEMS material. The Young's modulus of copper and nickel are 120 and 220 GPa, respectively. The ultimate strengths of annealed copper and nickel are 215 and 400 MPa, respectively. The LSP model can be better validated when the LSP effects of copper and nickel are compared.

Copper foils of 90-micron thickness and nickel foils of 120-micron thickness were used in LSP experiments. The samples were adhesively attached to bulk copper columns for rigid support and easy handling. The samples were polished and the sample size was about 8 mm square. To apply the coating, a thin layer of high vacuum grease (about 10 microns) was spread evenly on the polished sample surface, and the coating material, aluminum foil of 25 microns thick, which was chosen for its relatively low threshold of vaporization, is then tightly pressed onto the grease. The sample was placed in a shallow container filled with distilled water around 3 mm above the sample. A frequency tripled Q-switched Nd:YAG laser in TEM_{00} mode was used, the pulse duration was 50 ns, and pulse repetition rate could vary between 1 KHz to 20 KHz. Laser beam diameter is 12 microns. After shock processing, the coating layer and the vacuum grease were manually removed. Pulse number at each location was varied from 1 to 6 at 1 KHz repetition rate, and pulse energy was varied from 160 µJ to 240 µJ corresponding to laser intensity of 2.83 to 4.24 GW/cm^2. LSP at individual locations (similar to drilling) and overlapped locations (similar to grooving) was carried out. The geometry of the shocked region was observed and measured using optical microscope, SEM, and optical profiler.

The space- and time-dependent shock pressure was solved numerically based on the equations described in Section 2, and used as the loading for the subsequent stress/strain analysis. As seen, these equations are coupled, non-linear, and include several integrals. They were numerically solved using Matlab Simulink toolbox. The same constitutive relations as in (Zhang and Yao, 2000a) are used in the stress/strain analysis, in which work hardening, strain rate and pressure effects on yield strength are considered assuming room temperature. This is reasonable because only the coating is vaporized and minimal thermal effects are felt by the sample. A commercial FEM code, ABAQUS, is used for the stress/strain analysis as a dynamic implicit nonlinear process. First, axisymmetric modeling was carried out to compare the effects of the current shock pressure model with the previous model on deformation (Zhang and Yao, 2000a) assuming semi-infinity in geometry. Single and multiple pulses at individual locations were simulated. Secondly, 3D simulation was carried out assuming finite geometry (100 microns in thickness, 1 mm in width, and 2 mm in length). Pulses at overlapped locations with 50 micron spacing were simulated. Shocks are applied on the top surface along a narrow strip in the width direction. The bottom surface is fixed in position, while all the other side surfaces are set traction free.

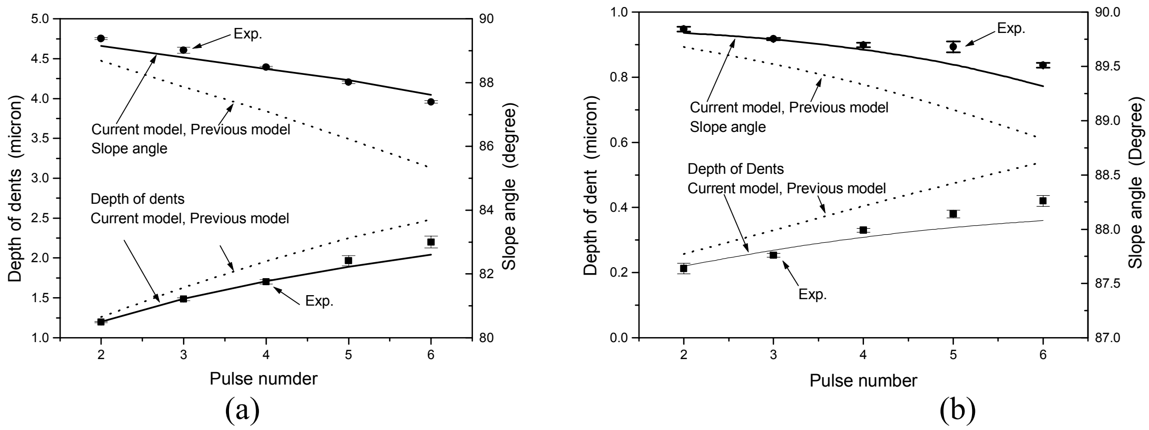

Figure 2 Dent geometry comparisons between current model and previous model (Zhang and Yao, 2000a), (a) copper, and (b) nickel. $E = 220$ μJ, $I = 3.89$ GW/cm^2, $AP = 0.5$, $\alpha = 0.2$.

4. Deformation Geometry and Validation of Current LSP Model

Micro scale LSP can induce plastic deformation on metal target as evidenced by dented geometry on the target surface (Zhang and Yao, 2000a). SEM observations have shown that the dent was due to shock pressure and not due to thermal effects. To quantitatively characterize the deformation, an interferometry based optical profilometer with a vertical resolution of 3 nm was used to profile deformed regions. Fig. 3(a) and (b) show the variation of dent depth and slope angle with the increase of pulse number at $E = 220$ μJ (3.89 GW/cm^2) for copper and nickel samples, respectively. The slope angle is defined as the angle between the surface normal and the average tangential line of the dent slope. Each experimental data point is the average of more than three dents and the error bar represents standard deviation. Simulation results of current and previous shock pressure model (Zhang and Yao, 2000a) are also superposed. The stress/strain analysis of the simulation is the same as reported in Zhang and Yao (2000a).

The current model agrees well with the experimental results while the previous model overestimates the dent depth especially at the larger number of pulses. This is primarily due to the fact that the previous model overestimated the shock pressure duration by neglecting the radial and axial expansions of the plasma (Fig. 5 (b)). When the number of pulses increases, the effect of such overestimation accumulates. This explains why the discrepancy gets larger with the number of pulses. The discrepancy in the slope angle can be similarly explained. Simulations and experiments under a wide range of other conditions showed similar trends. In summary, the current model gives better predictions of the deformation geometry than the previous model for two materials that have different mechanical properties.

5. Transient Phenomena of Water-Plasma-Coating Interaction

With the validation of the model in Section 3, more numerical results are extracted from the solution to the shock pressure model to help understand a number of transient phenomena. Fig. 3(a) compares the expansion speed of plasma (U_{pL}, U_{pR}) with the particle velocities of water and copper (U_{sw}, U_{sm}), in response to plasma absorbed laser intensity I_p=4 GW/cm^2. Please note the laser intensity profile normalized to the peak intensity is shown in Fig. 3(c). It is seen from Fig. 3(a) that the particle velocity of water is more than 10 times that of the target metal. The significant difference in U_{sw} and U_{sm} (the same as the coating material particle velocity U_c) can be explained by examining Fig. 3(b), which shows the shock pressure increase of water (confining medium), aluminum (coating layer), copper and nickel (target material), with the increase of particle velocity based on the Hugniot relations (Eqs. 1 to 4). It is clear from Fig. 3(b) that the particle velocity of water should be much larger than the particle velocity of the coating material. Please note the results (Fig. 3(b)) reflect the material properties and are independent of external effects.

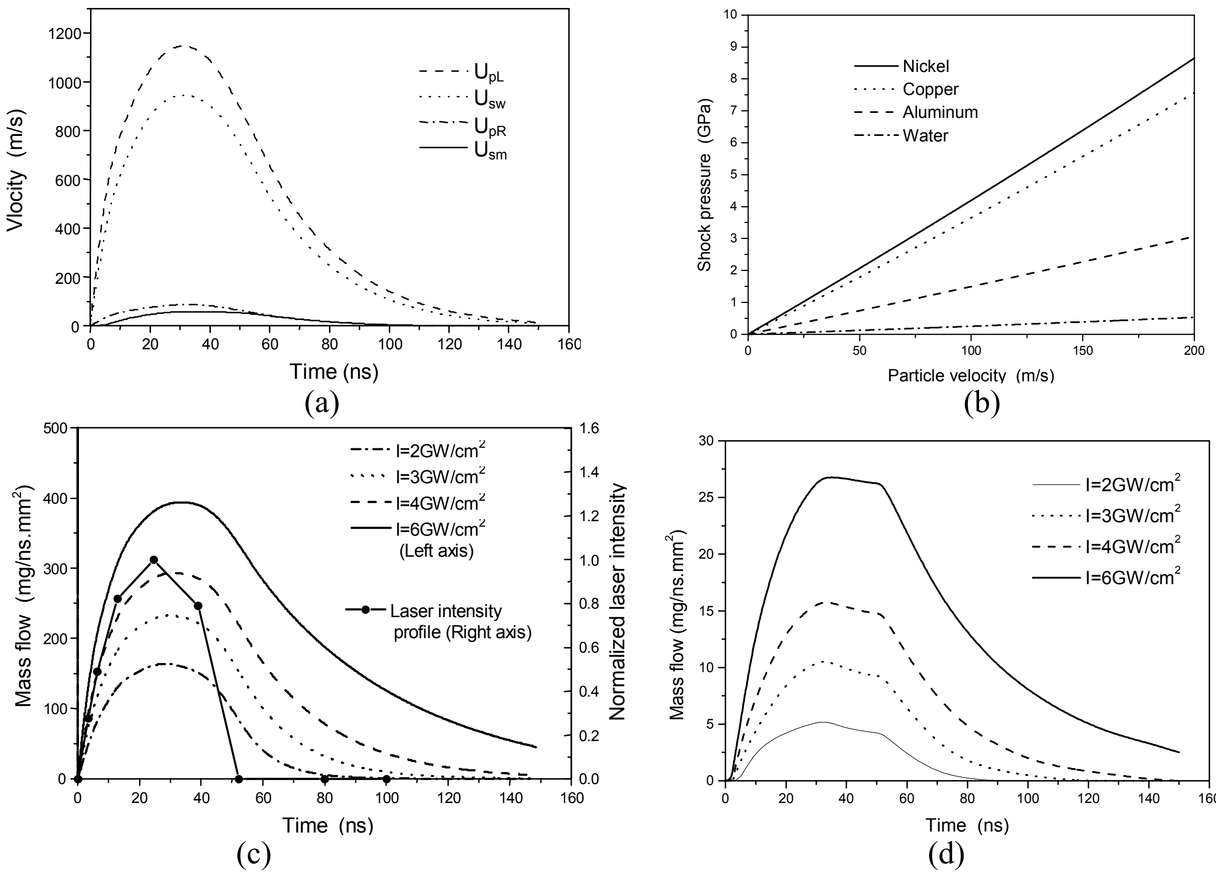

Fig. 3 (a) Comparison of expansion speed of plasma and particle velocity of copper and water; (b) Hugniot curves of nickel, copper, aluminum and water; (c) Mass flow from water to plasma; and (d) Mass flow from coating layer to plasma

From Fig. 3(a) it is also observed that U_{pl}>U_{sw} and U_{pR}>U_{sm}, and the differences decay to zero as time lapses. The difference between plasma expansion speed and water/target particle velocity indicates that mass flow exists from water and coating layer to plasma. Mass flow evolutions at four representative laser intensities are shown in Fig. 3(c) and (d) for water and the coating layer, respectively. Normalized laser intensity profile is superposed in Fig. 3(c) to illustrate that even after the laser pulse is off, there is still mass flow from water into plasma and the mass flow peaks after laser intensity peaks. The reason is that mass flow from water into plasma is caused by water breakdown, which is due to the combined effects of laser and plasma irradiation. Even after the laser pulse is off, the plasma irradiation sustains the mass flow for a period of time until the plasma cools down. As laser intensity increases, plasma accumulates more energy to irradiate. This is why it takes longer for the mass flow to peak when laser intensity increases.

The mass flow from the coating layer into plasma shows similar patterns and is about one order of magnitude lower than the mass flow from water to plasma. It's interesting to note that mass flow from the coating layer shows a plateau after the mass flow peaks, while the mass flow of water has a much smoother transition to zero values. The plateau is due to the different energy absorption of metal and water to laser and plasma irradiation. The plasma irradiation is primarily in the extreme ultraviolet (Root, et al., 1979). At such short wavelengths (<200nm), multi-photon ionization mechanism of water breakdown is dominant. As laser intensity weakens after t = 30 ns (Fig. 3(c)), the deep UV irradiation weakens, thus mass flow from water has a smooth transition with the same trend as the laser intensity. However, the total irradiation energy to the coating layer doesn't change much because plasma has accumulated enough energy and decays much slower than the laser intensity. And metals at high temperatures absorb strongly almost all the irradiation energy. This caused the plateau in Fig. 3(d).

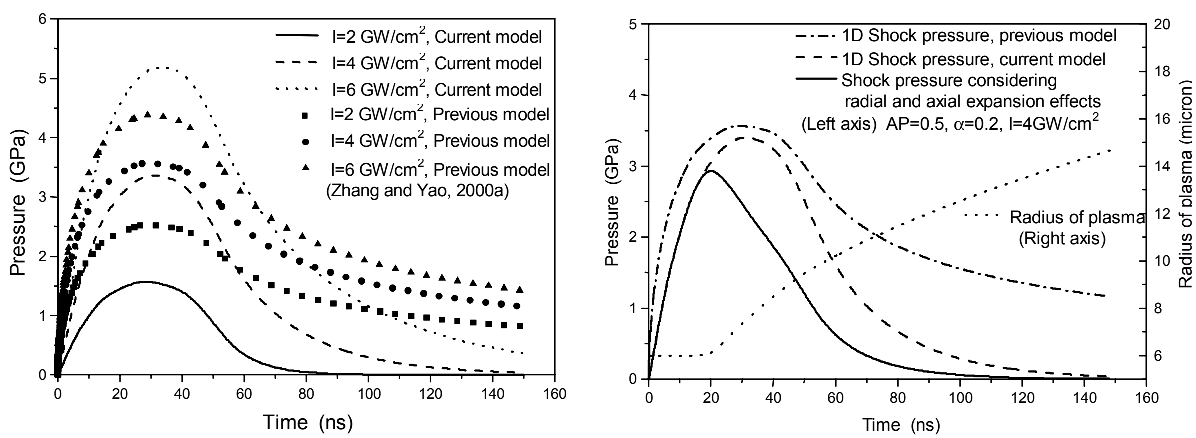

Fig. 4 (a) Shock pressure comparison between current model and previous model; and (b) Considerations of radial and axial expansion effects

Fig. 4(a) compares the 1D shock pressure determined using the current model and previous model (Zhang and Yao, 2000a). The previous model assumed that a constant fraction $\alpha = 0.2$ of plasma energy is used to increase the shock pressure during the expansion of the plasma. In the current model such conversion is inherently considered in the energy balance relations. As seen, the previous model determined a higher peak pressure at laser intensity of 2 GW/cm^2, a comparable value at 4 GW/cm^2, and a lower value at 6 GW/cm^2 than the current model. This is indicative of the shortcoming of using a constant value of α for different laser intensities in the previous model. As the energy level increases, the plasma tends to expand faster but experiences a higher level of resistance by water. As a result, the plasma spends a larger fraction of its internal energy on pressure increases and thus a larger value of α should have been used to account for this effect. The pressures recover to zero values faster in the current model than in the previous model. The reason is that in the current model, plasma energy is used for the breakdown of water and target material besides the expansion of plasma, while in the previous model only the 1D expansion of plasma was considered.

For laser beam size of micron scale, the radial and axial expansion effects on plasma must be accounted for. Eq. 16 was used to calculate the final shock load used in stress analysis. The temporal evolution of shock pressure and the radius of plasma at laser intensity of 4 GW/cm^2 are shown in Fig. 4(b). The radius of plasma is constant until the rarefaction wave merges at the center of the laser beam at about 20 ns. After that, a non-linear increase of plasma radius occurs. The shock pressure decreases after the rarefaction wave merges at the beam center according to power laws shown in Eq. 16. Obviously the shock pressure considering plasma expansion is more realistic and more suited for micro-scale LSP.

6. Three-dimensional Stress/Strain Analysis with Finite Geometry

Axisymmetric stress/strain analysis was conducted for micro-scale LSP at individual locations (Zhang and Yao, 2000a & b), in which semi-infinite geometry was also assumed. Such analysis results are used in Fig. 2 of this paper to compare with experimental measurements. For LSP overlapped locations, 3D stress/strain analysis is necessary. In addition, for complex geometry and for small-scale specimen, the semi-infinite geometry assumption needs to be removed.

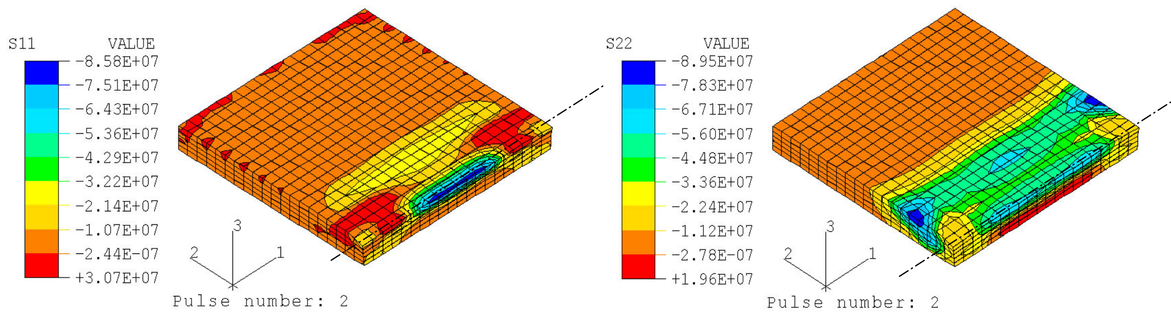

(a) (b)

Figure 5 Residual stress distribution of laser shock processed copper plate. (a) S11, and (b) S22. A series of successive shocks (with spacing of 50 microns) is applied along the centerline (shown in dotted line) of the 1mm by 2mm by 0.1 mm copper plate. Only half of the plate is shown due to symmetry. 2 pulses at each location with pulse energy 220 μJ.

Fig. 5 (a) and (b) illustrate typical residual stress distributions of *S11* (along laser scanning direction) and *S22* (vertical to laser scanning direction), respectively. Two observations can be made. First, the stress state at the edge areas is more complex than that in the interior area. This is obviously due to the effect of finite geometry. Typically less resistance to deformation is experienced at the edge areas. The residual stress state at the edge areas has significant influence on crack initiation and propagation. Secondly, *S22* is more uniformly distributed than *S11*. Fig. 5 (b) shows that LSP induced an area of surface compressive residual stresses perpendicular to the scanning direction, and the area extends 300 microns from the centerline. The maximum compressive stress is close to –90 MPa. If the specimen experiences a periodic load along the *S22* direction, the surface compressive residual stress will help improve its fatigue life.

Edge and finite size effects are important for practical applications because cracks usually initiate from the edge. Detrimental edge effects should be avoided and 3D simulation offers very valuable guidance for this purpose.

7.Conclusions

A new model of shock pressure considering mass, energy and momentum conservation is formulated, in which plasma is modeled as laser supported combustion wave and its spatial expansion effects are accounted for. The solution to the model enables better prediction of LSP induced deformation and at the same time provides valuable information on process transiency. 3D stress/strain analysis is carried out and the finite size and specific geometry effects in practical LSP are explained.

Acknowledgements

Financial support from NSF under grant DMI-9813453 and equipment support from ESI are gratefully acknowledged.

References

Assay, James R., and Shahinpoor, Mohsen, 1992, High-pressure Shock Compression of Solids, New York, Springer-Verlag, 1992, pp. 78-82.

Berthe, L., et al., 1998, "Experimental Study of the Transmission of Breakdown Plasma Generated During Laser Shock Processing," *The European Physical Journal Applied Physics*, 1998, Vol. 3, pp 215-218.

Clauer, A. H., et al., 1981, "Effects of Laser Induced Shock Waves on Metals," Shock Waves and High Strain Phenomena in Metals-Concepts and Applications, New York, Plenum, 1981, pp. 675-702.

Fabbro, R., et al., 1990, "Physical Study of Laser-produced Plasma in Confined Geometry," *J. Appl. Phys.*, July, 1990, Vol. 68(2), pp. 775-784.

Meyers, Marc A., and Murr, L. E., 1981, Shock Waves and High-Strain-Rate Phenomena in Metals, New York, Plenum Press, 1981, pp. 487-530,1048.

Pirri, A. N., et al., 1978, "Plasma Energy Transfer to Metal Surfaces Irradiated by Pulsed Lasers", *AIAA Journal*, Vol. 16, No. 12, pp.1296-1304.

Peyre, P., at al., 1995, "Laser Induced Shock Waves as Surface Treatment for 7075-T7351 Aluminum Alloy," *Surf. Engng.*, 1995, Vol. 11, pp. 47-52.

Root, Robert G., 1989, "Modeling of Post-Breakdown Phenomena," Laser Induced Plasmas and Application, New York, Marcel Dekker, Inc., 1989, pp. 95-99.

Simons, Girard. A., 1984, "Momentum Transfer to a Surface When Irradiated by a High-Power Laser," *AIAA Journal*, Vol. 22, No. 9, pp.1275-1280.

Vogel, Alfred, et al., 1996, "Plasma Formation in Water by Picosecond and Nanosecond Nd:YAG Laser Pulses," *IEEE Journal of Selected Topics in Quantum Electronics*, Vol. 2, No. 4, Dec., 1996, pp. 847-871.

Zhang, Wenwu and Yao, Y. Lawrence, 2000a, "Improvement of Laser Induced Residual Stress Distributions via Shock Waves," *ICALEO'2000, Laser Material Processing*, Vol. 89, pp. E183-192.

Zhang, Wenwu and Yao, Y. Lawrence, 2000b, "Micro Scale Laser Shock Processing of Metallic Components," *ASME Journal of Manufacturing Science and Engineering*, submitted.

Meet the authors

Wenwu Zhang is currently a Ph.D. candidate and Y. Lawrence Yao an Associate Professor in the Department of Mechanical Engineering at Columbia University, where Yao also directs the Manufacturing Engineering Program. Yao has a Ph.D. from Univ. of Wisconsin-Madison.